university of groningen

faculty of science and engineering

DAQ Simulation for the $\overline{\text{P}}$ANDA Experiment (phase 1)

Jisk Knijpstra

university of groningen

faculty of science and engineering

DAQ Simulation for the $\overline{\text{P}}$ANDA Experiment (phase 1)

Master's Thesis

To fulfill the requirements for the degree of
Master of Science in Physics (track: *Quantum Universe*)
at the University of Groningen under the supervision of
Dr. M. Kavatsyuk
and
Dr. K.A.M. de Bruyn

Jisk Knijpstra

March 27, 2023

Contents

1 Introduction

$\overline{\mathrm{P}}$ANDA (anti-**P**roton **AN**nihilations at **DA**rmstadt) is a planned hadron physics experiment. Exploiting high-intensity antiproton-proton annihilations, $\overline{\mathrm{P}}$ANDA will be a valuable tool to gain insight into fundamental questions regarding the interactions between coloured particles, mediated by the strong force. Why do quarks and gluons never appear as singlets, but always in some colourless combination? How do baryons get their masses, of which only some 2% is generated by the Higgs mechanism? Do there exist exotic hadronic states such as quark molecules, glueballs and hybrids as predicted by the standard model theory of quantum chromodynamics? These are some fundamental questions $\overline{\mathrm{P}}$ANDA will help to address.

One of the unique features of the $\overline{\mathrm{P}}$ANDA experiment, is that data acquisition will be performed with a triggerless data acquisition system, requiring software to perform event reconstruction in real-time. To obtain a manageable data rate, it is necessary to implement event-selection algorithms to discard uninteresting events. This poses challenges specific to the physics of the decay channels of interest. For realistic detector simulation at high event rates, time-based simulation mode was developed. There is still work to be done in adapting the existing simulation software to time-based mode, especially in the domain of charged track reconstruction.

In this work, full simulations of five different physics channels are performed, and methods to improve their reconstruction are offered.

1.1 Thesis outline

In chapter 2, an overview of the experimental facilites is given, along with a description of the physics programme and the $\overline{\mathrm{P}}$ANDA data acquisition system.
In chapter 3, the PandaRoot simulation environment is described, along with the time-based simulation mode and an the physics channels that are studied in this work. In chapter 4, results obtained from simulations are presented. Each of the subsections concerns a different type of physics channel. In the first subsection, the so-called Active Time parameter in time-based mode is optimised. In the second a method is presented to improve reconstruction of channels containing electrons or positrons in their final states. In the last subsection, reconstruction of hyperons is improved by supplementing the standard reconstruction algorithms with a secondary track finding algorithm. In chapter 5, a summary and conclusions are given.

2 Experimental facilities

2.1 The $\overline{\text{P}}$ANDA experiment at FAIR

$\overline{\text{P}}$ANDA is one of the four planned experiment at the new FAIR accelerator complex at GSI in Darmstadt, Germany. FAIR (**F**acility for **A**ntiproton and **I**on **R**esearch) is currently under construction and will enable fundamental physics research exploiting ion and antiproton beams [2]. Existing accelerators at GSI will be augmented by the new ring accelerators and experiments as shown in figure 2.1.

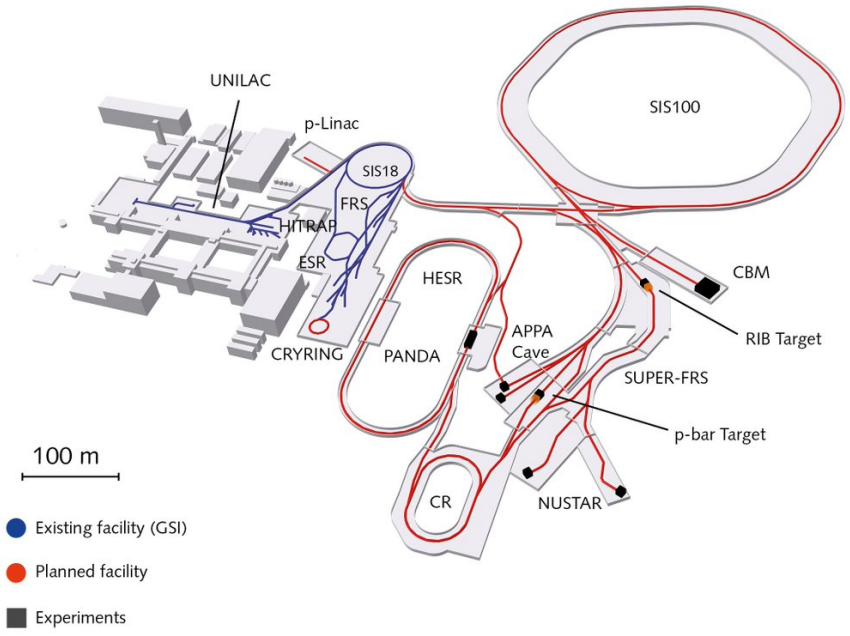

Figure 2.1: Design of the planned FAIR (Facility for Antiproton and Ion Research) [2].

The experiments each represent one of the four science pillars of FAIR: atomic and plasma Physics (APPA), compressed baryonic matter (CBM), nuclear structure and astrophysics (NUSTAR), and hadron and hypernuclear physics ($\overline{\text{P}}$ANDA). The superconducting heavy ion synchrotron SIS100 will accelerate heavy ions or protons, creating an intense primary beam. Aided by proton injections from the linear proton accelerator (p-Linac), the primary beam (up to $p_{\text{p}} = 30\,\text{GeV/c}$ for protons) can be impinged on production targets to produce a secondary beam of antiprotons (pertinent to $\overline{\text{P}}$ANDA), or of exotic nuclei for other experiments. The produced antiprotons are collected and pre-cooled in the Collector Ring (CR) before being injected into the High energy Storage Ring (HESR).

The HESR, shown in figure 2.2, will utilise phase space cooling techniques to control the beam emittance [3]. The electron cooler injects electrons parallel to the antiproton beam. The antiprotons lose momentum through scattering processes, reducing the momentum spread in the beam. Additionally stochastic cooling is performed, which essentially entails measuring and subsequently correcting individual particles in bunches electromagnetically over

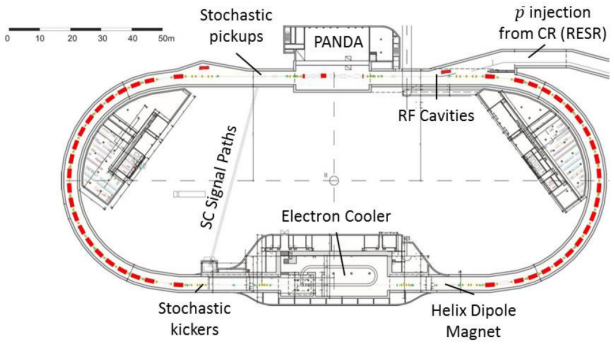

Figure 2.2: Design of the High Energy Storage Ring [4].

multiple iterations. With the aforementioned techniques, it is possible to adjust the beam luminosity and momentum resolution. The HESR is designed to have two modes of operation: [5]

- High Luminosity (HL) mode, with a beam momentum of $p = 1.5 - 15\,\mathrm{GeV/c}$, momentum spread $\sigma_p/p \sim 10^{-4}$, and a peak luminosity of $2 \times 10^{32}\,\mathrm{cm^{-2}s^{-1}}$.
- High Resolution (HR) mode, with a beam momentum of $p = 1.5 - 8.9\,\mathrm{GeV/c}$, momentum spread $\sigma_p/p \leq 4 \times 10^{-5}$, and a peak luminosity of $2 \times 10^{31}\,\mathrm{cm^{-2}s^{-1}}$.

The number of antiprotons stored in the HESR at any time will be up to the order of 10^{11}.

In the current design of the experiment, $\overline{\mathrm{P}}$ANDA is planned to operate in increasingly complex configurations, referred to as phases. During phase 1 the maximum event rate will not yet be $20\,\mathrm{MHz}$, but will be limited to $2\,\mathrm{MHz}$. In later phases, after upgrades of the HESR and the $\overline{\mathrm{P}}$ANDA detector, the available beam luminosity will be higher allowing for greater event rates.

2.2 The $\overline{\mathrm{P}}$ANDA detector

The detector, designed as shown in figure 2.3, consists of two main parts: a barrel part, or target spectrometer (TS), and a forward part, or forward spectrometer (FS). This configuration yields the detector the important distinguishing feature of covering almost the full solid angle (near-4π coverage). The target spectrometer is built around the interaction point. This is where the beam of antiprotons collides with a stationary proton target. This target may take on different forms in different phases of the experiment: during phase-1, a cluster-jet target will be used. During later phases, a hydrogen pellet target will be installed to cope with the increased beam luminosity [6]. Moreover, the TS contains the central tracking system as well as an electromagnetic calorimeter and a number of PID detectors, and is enveloped by a superconducting solenoid magnet. The magnet induces an approximately homogenous magnetic field parallel to the beam direction, causing charged particles to follow curved tracks inside the detector(s). By measuring a track's radius of curvature in the tracking detectors, the corresponding particle's transverse momentum can be inferred. Equating the Lorentz force exerted perpendicularly to the particle's direction of motion, $qv_\perp B$, to the centripetal force $\frac{mv_\perp^2}{R}$, one obtains a relation between the transverse momentum $p_\perp$ and the radius of curvature R:

$$p_\perp = qBR, \tag{2.1}$$

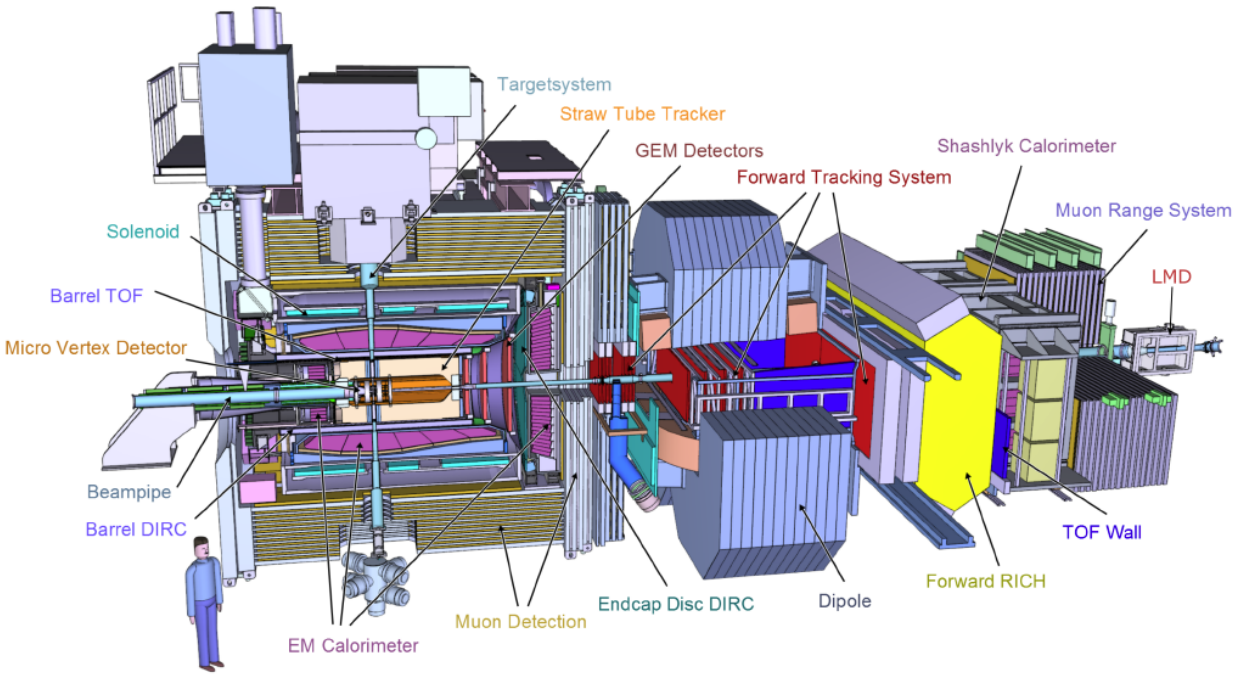

Figure 2.3: A cross section view of the $\overline{\mathrm{P}}$ANDA detector [2].

where q denotes the particle's charge, and B the magnetic field strength. Note that the sign of the particle's charge can be inferred from the direction of its track's curvature. The study of charged particle tracks is commonly referred to simply as "tracking", and charged particle tracks themselves as "tracks". From hereon I will use this shorthand to refer to charged particle track detectors as "tracking detectors" and to charged track reconstruction algorithms as "tracking algorithms".

2.2.1 Subdetector systems

The TS tracking system consists of three types of tracking detectors. Located closest to the interaction point is the **Micro Vertex Detector** (**MVD**), which can precisely locate the interaction vertex and decay vertices of short-lived particles such as hyperons or charmed mesons. Featuring fine granular silicon pixel detectors and double-sided silicon strip detectors, the spatial resolution of the MVD will be about $100\,\mu\mathrm{m}$ in the longitudinal direction and $35\,\mu\mathrm{m}$ in the transverse direction [7]. With these qualities, MVD information is especially valuable for transverse momentum reconstruction of tracks.

Enveloping the MVD is a **Straw Tube Tracker** (**STT**). The STT comprises 4636 cylindrically packed straw tubes. They are gas-filled tubes with a central wire, and function in the same way as an ionisation chamber: a potential difference of some kilovolts is applied between the anode wire and the cathode layer. When a charged particles ionise the gas inside a tube, free electrons accelerate towards the anode wire, resulting in a signal. From the drift time, it can only be deduced at what radial distance from the wire the ionisation took place. Therefore STT hit information consists of this radial distance, called the *isochrone radius*, describing a cylindrical surface containing all possible positions of the ionising particle. The STT will have a spatial resolution of $150\,\mu\mathrm{m}$ in the transverse direction and at most $3\,\mathrm{mm}$ in the longitudinal

direction. The green coloured straw tubes in figure 2.5 are aligned with the beam axis (i.e. z-axis), while the blue and red marked straws are skewed relative to the beam axis by $2.9°$ and $-2.9°$, respectively. There is a vertical gap to make space for the target system. Besides tracking, the STT functions as a PID detector to distinguish lower energy protons, kaons and pions, by measuring their energy loss in the medium, $-dE/dx$.

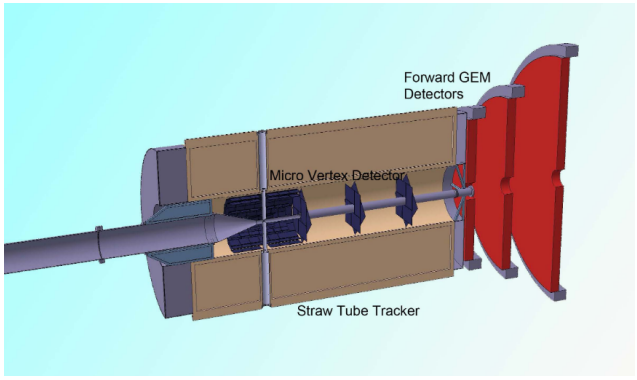

Figure 2.4: Schematic cross section of the tracking detectors in the target spectrometer [7].

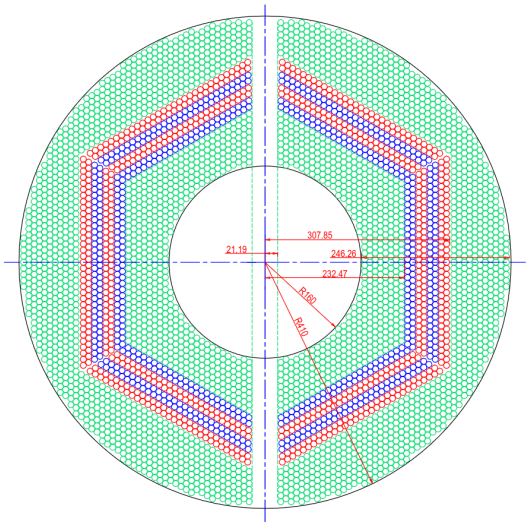

Figure 2.5: Schematic layout of the stray tubes in the STT, in xy-view. Image taken from [7].

For tracking in the forward direction at the boundary between the TS and the FS, **Gas Electron Multiplier (GEM)** stations will be installed (coloured red in figure 2.4). Incoming particles can be detected when they initiate an electron cascade inside the detector volume, which is filled with a gas mixture. The induced signal is amplified and read out on both the front and back sides of the disks.

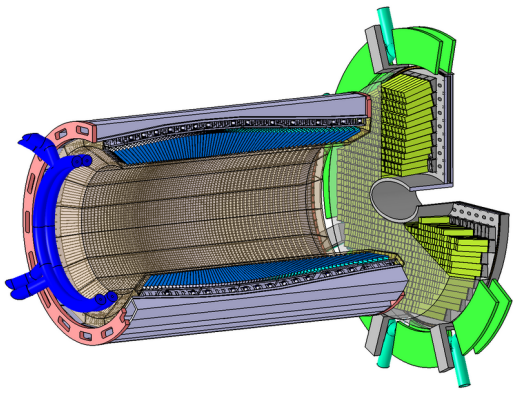

Figure 2.6: The barrel- and forward endcap EM calorimeters [8].

Besides tracking detectors, the TS contains a number of calorimeters and PID (particle identification) detectors. Rather than measuring momenta of charged particles, **electromagnetic calorimeters (EMCs)** are designed to measure energy depositions of photons and electrons. This is done by means of absorption in scintillation crystals (for the $\overline{\text{P}}$ANDA EMC lead tungstate ($PbWO_4$) was chosen). The TS EMC will consist of three separate parts located

in the barrel, the forward endcap and the backward endcap, respectively. The FS EMC has a shashlik design, comprising alternating layers of absorber material and scintillators. The TS EMC will comprise about $15\,700$ individual crystals. The reason that so many separate crystals are placed together is that electromagnetic particles, upon interacting with the scintillation material, will initiate particle showers which can extend out into multiple crystals. This greatly simplifies reconstruction of the primary particle compared to if the shower were contained in a large single crystal volume. The main challenge in reconstucting such a primary state is then to identify groups of EMC hits most likely to belong to one shower, called *clusters*.

In addition to the tracking- and EMC detectors described above, the $\overline{\mathrm{P}}$ANDA detector will contain an additional tracking system in the FS part as well as a number of PID detectors in both the TS and FS. As these detectors are not of particular relevance to this work and for the sake of brevity, I refer the interested reader to the article by G. Schepers et al. [9].

2.3 Physics programme

In a broad sense, the objective of the $\overline{\mathrm{P}}$ANDA experiment is to study QCD (quantum chromodynamics) in the confinement regime. Although QCD is a standard model theory, fundamental questions remain surrounding phenomena such as quark confinement, hadronic mass generation, and the possibile existence of exotic states of hadronic matter. Using $\bar{p}p$ annilihations, $\overline{\mathrm{P}}$ANDA aims to investigate these questions by precision measurements at medium-low energies, on the boundary between the perturbative and non-perturbative regimes of QCD. The physics programme can be summarised in four pillars, listed below.

Charm and Exotics
In addition to ordinary where hadrons occur as quark triplet states (baryons) and quark-antiquarks states (mesons), QCD in principle also allows more exotic bound quark states, as long as they are colourless. This would include states consisting more than three quarks (multiquarks), or states where both quarks and gluons contribute to the quantum numbers (hybrids), or even states that solely of gluons (glueballs). A number of unpredicted charmonium states have been observed in other experiments which exhibit properties of exotic hadrons [10]. The possibility of adjusting the beam momentum with high precision grants $\overline{\mathrm{P}}$ANDA the unique ability to measure energy-dependent cross-sections of narrow resonances at a range of centre of mass energies. This technique is called a resonance energy scan [11]. An advantage of $\overline{\mathrm{P}}$ANDA 's antiproton-proton annihilations is that states with exotic quantum numbers can be produced with relative ease. In e^+e^- colliders, in contrast, hadron creation necessarily involves a virtual photon which has quantum numbers $J^{PC} = 1^{--}$, strongly suppressing exotic states. It is this combination of precision and access to exotic quantum numbers that give $\overline{\mathrm{P}}$ANDA its unique ability to detect exotic hadronic states with the energy resolution necessary to clarify their nature.

Hyperons and Hypernuclei
A hyperon is a baryon containing at least one strange quark. The lightest one is the lambda baryon (Λ), which we will encounter later in this work in one of the simulation benchmark channels. With its $\bar{p}p$ annihilations, hyperon pairs can be formed at high cross-sections in the $\overline{\mathrm{P}}$ANDA experiment. An atomic nucleus containing at least one hyperon is what is called a

hypernucleus. The added strangeness degree of freedom gives these objects some interesting dynamics in how they are bound. Formation of hypernuclei will be studied at $\overline{\mathrm{P}}$ANDA with a special target.

Nucleon Structure
Much is unknown about the internal structure of the nucleon. The spatial distribution of electric charge and current inside hadrons can be described by electromagnetic form factors. In the $\overline{\mathrm{P}}$ANDA experiment, the Dalitz decays $\bar{p}p \to e^+e^-$ and $\bar{p}p \to \mu^+\mu^-$ will be measured to find the space-like and time-like EM form factors of the proton.

Hadrons in Matter
By letting the antiproton beam impinge on a nuclear target, $\overline{\mathrm{P}}$ANDA will be used to study how nuclear forces arise from QCD and how properties of hadrons change when placed in a medium. Studying the nuclear potential could, among other things, contribute to our understanding of neutron stars.

2.4 Data acquisition

With expected interaction rates of up to $20\,\mathrm{MHz}$ and a highly diverse physics programme, the $\overline{\mathrm{P}}$ANDA data acquisition system (DAQ) is subject to stringent constraints in terms of reconstruction precision. In high luminosity mode, the raw data rate is projected to be in the order of hundreds of gigabytes per second, and strong event pileup is expected. Storing such large amounts of data permanently is not feasible. Therefore a data reduction factor of at least 100 by the DAQ is envisioned. In this data reduction process, the principal challenge is to separate those events which are of interest for physics analysis from uninteresting events (i.e. background and possible decays that we do not wish to study). The interaction cross sections of the signal events is in most cases several orders of magnitude smaller than the background cross section at the same centre of mass energy [12]. The challenge of separating signal from background events is further complicated by the similarity of their decay topologies (i.e. leaving hard to distinguish detector signatures), making the search for some decays akin to searching for a needle in a haystack.

Data reduction and event selection are conventionally handled with hardware triggers. However, in order to cope with the abovementioned constraints of precision for the $\overline{\mathrm{P}}$ANDA experiment, it was deemed necessary to implement a more refined trigger system fully based on software. Such a system is commonly referred to as a **triggerless DAQ system** (**tDAQ**). The tDAQ system takes in the combined time-ordered data stream from all subdetectors (this task is performed with a protocol called SODANET), and performs online (real-time) track/cluster reconstruction and event building. Then, finally, the resulting event candidates with PID information are passed to the software trigger. By comparing these event candidates with the signatures of the physics channels of interest, set in advance for each run of the experiment, the software trigger finally determines which events to discard, and writes the remaining events to storage [13].

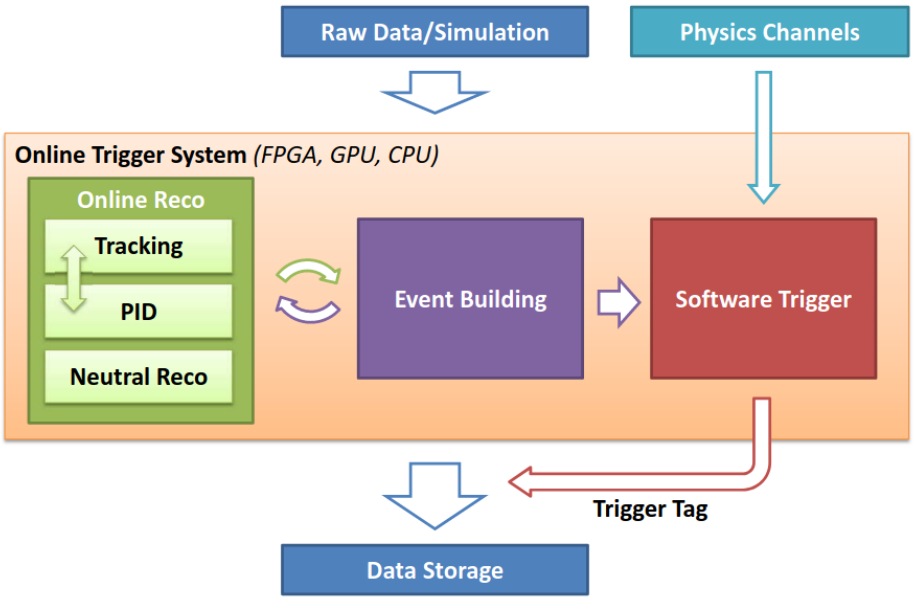

Figure 2.7: Visualisation of the data flow in the online trigger system of the $\overline{\text{P}}$ANDA tDAQ [13].

3 Simulations in PandaRoot

PandaRoot is a software framework dedicated specifically to Monte Carlo simulations of the $\overline{\text{P}}$ANDA experiment [14]. Developing a realistic simulation environment is important to aid development and optimisation of subdetector systems and, the central focus of this work, algorithms for the tDAQ system to perform track/cluster reconstruction, PID and physics analysis tasks.

Figure 3.1: The PandaRoot logo.

PandaRoot provides a central environment in which various tasks and simulation stages can be performed. The stages of a PandaRoot simulation chain will be given in section 3.1. PandaRoot is an extension of FairRoot, a framework containing base packages suited for simulation of experiments at FAIR, which is in turn based on the object-oriented data-analysis framework ROOT, developed at CERN in the `C++` programming language. In addition, PandaRoot makes use of several external software packages for event generation and propagation such as EvtGen and GEANT4.

3.1 Simulation chain

A full simulation chain in PandaRoot consists of five main stages, which are described below in the order in which they are executed. The word chain is used in this term, because each link (i.e. each stage or its corresponding task) requires the complete data output of the previous task as its input. The order is as follows:

1. **Simulation**
   In the simulation stage, physics events are generated and propagated. An *event* here signifies a set of primary particles (i.e. direct products of an $\bar{p}p$ annihilation and their decay products) with certain four-momentum vectors and vertex positions, pseudo-randomly generated according to physical models and some input parameters such as centre-of-mass energy and physics channel. This constitutes the *generation* part of the simulation stage and can be carried out by a number of external software packages, so-called generators. In this work, the generator EvtGen [15] was used for generating signal events, while for background events the FTF generator [16] was used. Next, the final states of the primary particles from the generator are taken as input by a propagator (GEANT3 or GEANT4). The propagator simulates the trajectory of the primary particles through the detector geometry and magnetic field. This is done iteratively with a certain step size, at each step generating a next state based on a physics model. Taking into account the possibility of interaction between a particle and the medium it is in, secondary particles can be created. Finally the simulation stage outputs a set of events containing simulated particle paths, called *MC tracks*. An MC track is essentially a collection of *MC points* belonging to one simulated particle, where MC points are the states of the particle at each iteration of the propagation process. Therefore MC tracks

contain all information about an event that can be known, and this information (called *MCTruth*) can be used later for comparison to evaluate the accuracy or efficiency of reconstructed events.

2. **Digitisation**
   In the digitisation stage, the response of subdetectors to the previously generated particles is simulated. Essentially, MC points are converted into MC hits, taking into account the specific hit resolutions of each subdetector. The output of the digitisation stage consists of digitised hits, sometimes called *digis*, which are no longer assigned to specific MC particles. This output is should closely resemble the real data coming from the detector electronics.

3. **Track Reconstruction**
   The remaining simulation stages concern the tasks of the online trigger system, i.e. to make track/cluster reconstructions out of the digitised detector data and attempt to recombine them to physics events. To reconstruct full tracks, digis from different subdetectors are combined. The digis are grouped together with pattern finding algorithms. This process is called track finding and produces *track candidates*, and gives a rough estimate of its track parameters (charge, momentum, etc.). In order to obtain a more accurate estimation of a track's parameters, additional track fitting can be done with a Kalman filter algorithm [17]. This algorithm uses the rough estimate of a track candidate's track parameters as initial parameters for an iterative fit (iterating through the track candidate's hits). An important aspect of this fitting procedure is how energy loss is modelled [18], which is not taken into account in the rough estimation. Kalman filtering is applied with a separate macro after track reconstruction, but is too computationally expensive for online processing. Unlike track hits, EMC digis are grouped into clusters, which have their own parameters such as cluster energy and angle.

4. **Particle identification**
   In the PID stage, the track candidates found in the previous stage are extrapolated into the PID detectors, and the track parameters are supplemented with pid information such as dE/dx, cherenkov angle and cluster energy. EMC clusters found to be uncorrelated to charged tracks are considered as neutral candidates. Based on this information, different algorithms in each PID detector construct a stable particle hypothesis for every charged candidate $k \in \{e, \mu, \pi, K, p\}$. A global PID probability $p(k)$ can be formulated for each hypothesis by combining the local PID probabilities $p_i(k)$ of each subdetector i [19].
   $$p(k) = \frac{\Pi_i p_i(k)}{\Sigma_j \Pi_i p_i(j)}. \tag{3.1}$$
   In the denominator, the probabilities of each particle type j are summed so that $p(k)$ is normalised.

5. **Analysis**
   Finally, event selection is done using the Rho package of PandaRoot. This entails combining particle candidates into physics events (i.e. reconstructing decay vertices by combinatorics, accounting for double counting effects), based on the PID probabilities of the candidates. Kinematic- and mass cuts can be applied by the user to refine event selection and reduce combinatorics. After full events have been reconstructed, physics

observables can be estimated from them, such as decay parameters or invariant masses of the particles.

3.2 Time-based simulation

In the conventional event-based simulation mode, full events at the digitisation level are processed one by one. The digitisation output data is structured such that the events are stored in a ROOT tree, containing branches corresponding to the different subdetectors, and each branch containing leaves with information about detector hits. Each event is fully described by one entry in the tree. This structure works under the assumption that events can be treated independently, i.e. that the time between events is greater than the time in which any of the subdetectors process their inputs. Sadly, this assumption does not hold when the interaction rate is as high as $\overline{\mathrm{P}}$ANDA's expected 2×10^7 events/s in HL mode, resulting in a mean time between events of $50\,\mathrm{ns}$. In this case, the order of detector signals reaching the DAQ does not necessarily follow the event order, but signals from different detectors can be mixed because some are 'slower' than others. See figure 3.2. Therefore, event times need to be deconvoluted. For this purpose, the structure of FairRoot was redesigned to allow time-ordering of events. In such a time-based simulation, all hits in a subdetector are assigned a timestamp according to a probability distribution. These timestamps are used as a basis for event-time reconstruction.

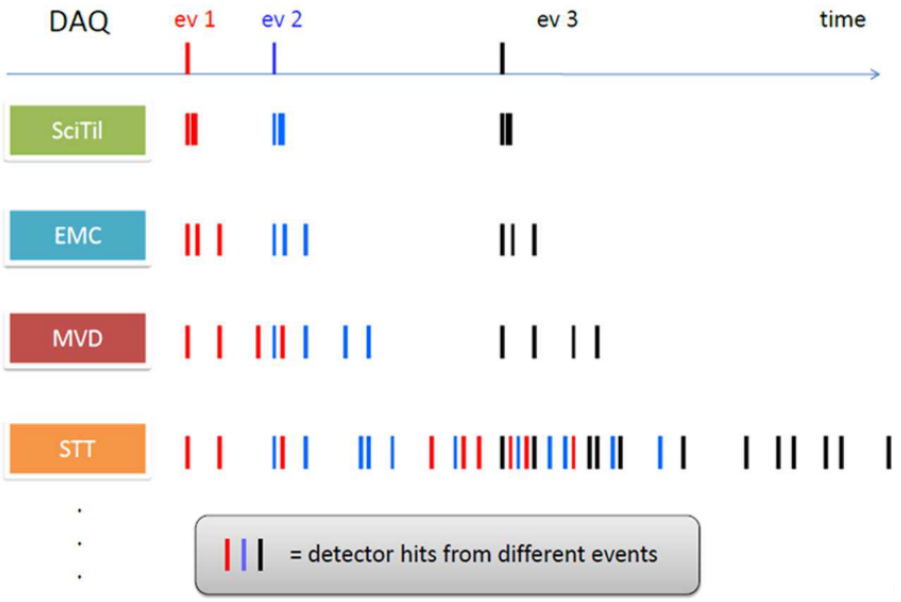

Figure 3.2: Timestamp structure for different subdetectors. Slower detectors such as the STT will see hits from separate events overlapping with each other. Image taken from [19].

The user can select manually to run a simulation in event-based or time-based mode. Currently, work is being done to adapt track reconstruction algorithms to time-based mode (see e.g. [22]). This is challenging because of the more complex data structure, but highly necessary for realistic detector simulation. Event-based simulation is inadequate at high interaction rates because event overlap and signal pileup are not accounted for.

3.3 Online filter task and benchmark channels

To reduce the amount of data to be processed, an online event filtering procedure is envisioned. This filtering would be performed before the final physics analysis and is based on just the estimates of track/cluster parameters of an event. This event filter has been implemented as a PandaRoot task, **PndFilter** [21]. The filter task makes use of selection cuts of certain features, selected for their distinguishable signal and background characteristics. See figure 6.17 on p.134 of Viktor Rodin's PhD thesis [21]. The user can set such conditions and the number of selection cuts manually.

Five benchmark channels are studied to gauge the performance of the DAQ simulations and the online filter. This combination of channels was selected for its broad coverage of aspects of the $\overline{\mathrm{P}}$ANDA physics programme [20]. Listed below are the five channels and the beam momenta at which they are simulated, as well as the corresponding centre-of-mass energies and approximate cross-sections of the primary interactions. With the target proton being stationaryand the antiproton having a momentum $p_{\bar{p}}$ in the laboratory frame of reference, the centre-of-mass energy is given (in natural units) by $E_{\mathrm{CM}} = \sqrt{2m_p^2 + 2m_p\sqrt{m_p^2 + p_{\bar{p}}^2}}$, where $m_p = 938.3\,\mathrm{MeV}$ is the proton rest mass.

1. $\bar{p}p \rightarrow J/\psi(\rightarrow \mu^+\mu^-)\pi^+\pi^-$
   at $p_{\bar{p}} = 6.988\,\mathrm{GeV/c}$, $E_{\mathrm{CM}} = 3.872\,\mathrm{GeV}$ and $\sigma = \mathcal{O}(50\,\mathrm{nb})$.

2. $\bar{p}p \rightarrow J/\psi(\rightarrow e^+e^-)\pi^+\pi^-$
   at $p_{\bar{p}} = 6.988\,\mathrm{GeV/c}$, $E_{\mathrm{CM}} = 3.872\,\mathrm{GeV}$ and $\sigma = \mathcal{O}(50\,\mathrm{nb})$.

3. $\bar{p}p \rightarrow e^+e^-$
   at $p_{\bar{p}} = 1.5\,\mathrm{GeV/c}$, $E_{\mathrm{CM}} = 2.256\,\mathrm{GeV}$ and $\sigma = \mathcal{O}(1\,\mathrm{nb})$.

4. $\bar{p}p \rightarrow e^+e^-\pi^0(\rightarrow \gamma\gamma)$
   at $p_{\bar{p}} = 1.5\,\mathrm{GeV/c}$, $E_{\mathrm{CM}} = 2.256\,\mathrm{GeV}$ and $\sigma = \mathcal{O}(10\,\mathrm{nb})$.

5. $\bar{p}p \rightarrow \Lambda^0(\rightarrow p\pi^-)\bar{\Lambda}^0(\rightarrow \bar{p}\pi^+)$
   at $p_{\bar{p}} = 1.641\,\mathrm{GeV/c}$, $E_{\mathrm{CM}} = 2.304\,\mathrm{GeV}$ and $\sigma = \mathcal{O}(100\,\mu\mathrm{b})$.

The goal of the online filter is to reduce the number of background events by two to three orders of magnitude. It also erroneously rejects some signal events. About $25\,\%$ to $67\,\%$ of signal events survive the filter depending on the channel, but this is considered acceptable if the background suppression goals are met.

The following selection criteria for each channel were chosen for their distinguishable signal and background signatures [21]:

(1) $J/\psi(\rightarrow \mu^+\mu^-)$. For this channel the penetration depth in the iron layers of the muon detector (MDT), L_{iron} is used. The criterion is $L_{\mathrm{iron}} > 40\,\mathrm{cm}$.

(2 – 4) $\bar{p}p \rightarrow \ldots e^+e^- \ldots$. These channels can be identified well with the EMC. The criterion used is the product of cluster polar angle θ_{cl} and cluster energy E_{cl}:
$E_{\mathrm{cl}} \times \theta_{\mathrm{cl}} > 0.7\,[\mathrm{GeV} \times \mathrm{rad}]$

(**5**) $\bar{p}p \rightarrow \Lambda^0\bar{\Lambda}^0$. The high initial background of this channel makes separating signal from background relatively difficult, requiring multiple selection cuts to sufficiently suppress the background:

- Primary proton track polar angle $\theta_{\text{proton}} < 0.5\,\text{rad}$.
- Polar angle between primary proton and pion $\theta_{p\pi} < 1\,\text{rad}$.
- Estimated polar angle of Λ $\theta_\Lambda < 0.45\,\text{rad}$.
- First Fox-Wolfram moment $FW_1 > 0.1$.
- Proton energy loss in the STT $dE/dx_{\text{STT}} > 8.5\,\text{a.u.}$
- Presence of GEM hits.

4 Results and analysis

In this section, results obtained from simulations of the benchmark channels are presented. Each subsection is concerned with one type of channel. In the first subsection, optimisation of the so-called active time parameter is done for the channel $\bar{p}p \to J/\psi(\to \mu^+\mu^-)\pi^+\pi^-$ in time-based mode. In the second subsection, the channels $\bar{p}p \to e^+e^-$, $\bar{p}p \to e^+e^-\pi^0(\to \gamma\gamma)$, and $\bar{p}p \to J/\psi(\to e^+e^-)\pi^+\pi^-$ are improved, also in time-based mode. The third subsection concerns the most challenging channel, $\bar{p}p \to \Lambda^0(\to p\pi^-)\bar{\Lambda}^0(\to \bar{p}\pi^+)$, which can be reconstructed better by introducing an additional tracking algorithm, but only in event-based mode. For all benchmark channels, full simulations from event generation to analysis were done. In the analysis stage, the complete decay tree of a channel is reconstructed. The reconstruction efficiency was gauged by inspecting the reconstructed invariant mass of the $\bar{p}p$ system or intermediate resonances for all events.

4.1 Optimisation of the active time parameter

In the event building stage, the active time is a parameter that sets a maximum on the difference in arrival time that may exist between consecutive digitised hits in order for the hits to be correlated by the algorithm. During the propagation stage in a time-based simulation, particles are simulated to travel through the detector medium, leaving hits in different subdetectors at different times. In order to reconstruct events accurately, the active time must be set accordingly. If it is set too low, the algorithm cannot correlate digis from different subdetectors that might have originated from the same interaction. If the active time is set too high, on the other hand, digis belonging to different interactions will be correlated more frequently.

The influence of the active time on the reconstruction efficiency was studied on the benchmark channel $\bar{p}p \to J/\psi(\to \mu^+\mu^-)\pi^+\pi^-$. Simulation and digitisation of 4000 signal events were done, and subsequently event reconstruction was done for a range of active time values between $1\,\mathrm{ns}$ and $1000\,\mathrm{ns}$. After the online filter and analysis stages, an invariant mass spectrum of the J/ψ resonance is obtained (one spectrum for each active time value). The invariant mass is calculated using the total energy and momenta of the final state particles of each event: $M_{\mu^+\mu^-} = \sqrt{E_{\text{tot}}^2 - |\vec{p}_{\text{tot}}|^2}$. The invariant mass spectra look like that in figure 4.1: a spectrum consisting of a peak centred at $3.1\,\mathrm{GeV}$ and a background contribution.

As for the efficiency of such a reconstruction, it can be defined as the ratio between the number of counts under the peak of the reconstructed invariant mass spectrum, and the number of simulated signal events:

$$\varepsilon_{\text{signal}} = N_{\text{reco}}/N_{\text{sim}}. \tag{4.1}$$

There is an inevitable uncertainty in N_{reco}, because the precise shape of the combinatorial background is not known. Nevertheless, the number of counts underneath the peak can be estimated by performing a Gaussian + polynomial fit in the peak region and computing the integral of the Gaussian part of the fitted function. See figure 4.2. Repeating this fitting procedure for all obtained invariant mass spectra, each corresponding to a unique active time value, the reconstruction efficiency can be calculated and plotted as a function of active time. This analysis was done for simulations at five different interaction rates, each represented by a different colour in figure 4.3. The error bars correspond to the systematic uncertainties due

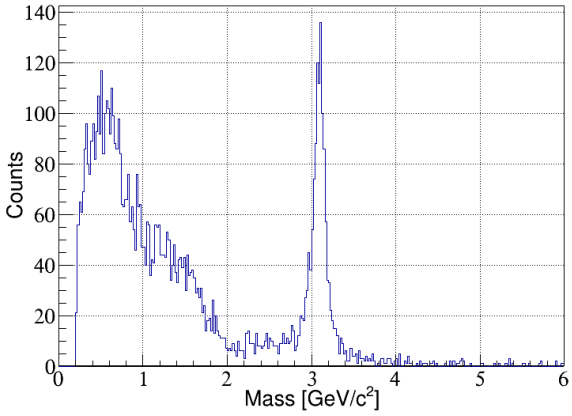

Figure 4.1: Obtained J/ψ invariant mass spectrum for an active time of $40\,\mathrm{ns}$ and an interaction rate of $2\,\mathrm{kHz}$ ($N_{\mathrm{entries}} = 6575$).

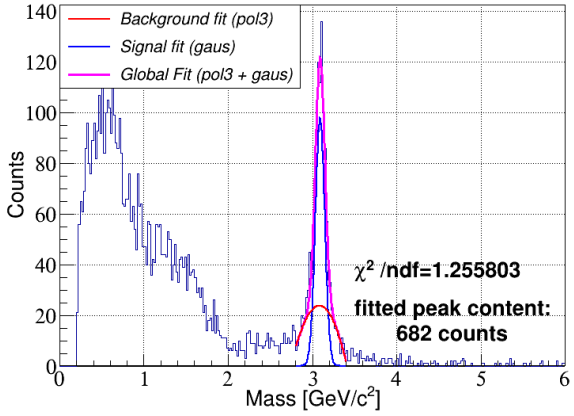

Figure 4.2: Fit of peak region by a Gaussian + third order polynomial. The number of signal counts is estimated by integrating the resulting Gaussian.

to the unresolved shape of the combinatorial background. The magnitudes of these uncertainties are equal to the difference in integrated peak counts obtained from each spectrum between a cubic- and a linear fit of the background. Statistical uncertainties have been ignored.

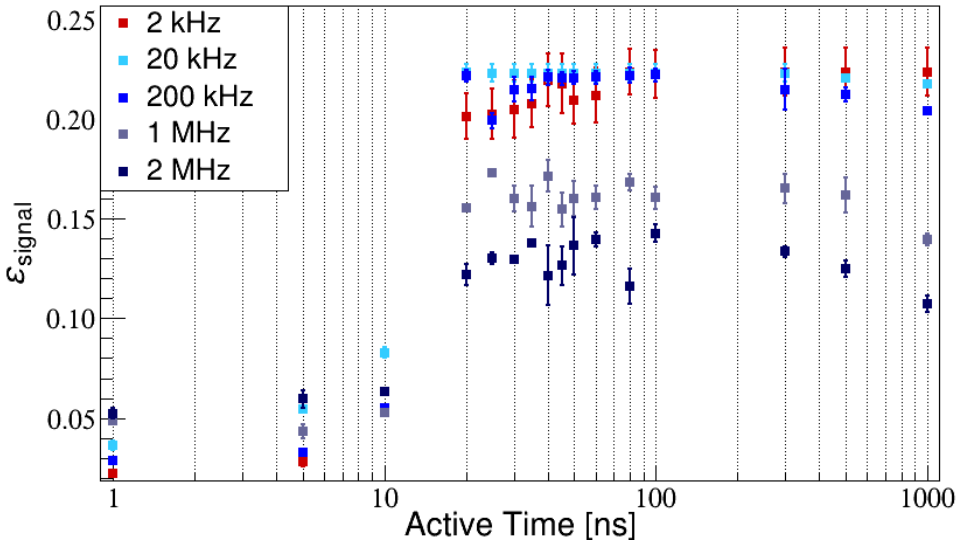

Figure 4.3: Reconstruction efficiency vs. active time for a range of interaction rates between $2\,\mathrm{kHz}$ and $2\,\mathrm{MHz}$. An interaction rate of $2\,\mathrm{MHz}$ corresponds to a mean time between interactions of $500\,\mathrm{ns}$

Clearly, reconstruction fails when the active time is set to too low values. Keeping in mind that the average (global) time difference of the first digis between the MVD and STT is about $15\,\mathrm{ns}$ [21] , it is not surprising that the reconstruction efficiency drops heavily for active time values lower than this value. Independent of interaction rate, the efficiency is optimal for an active time of some tens of nanoseconds. For active time values on the order of hundreds of

nanoseconds, the efficiency begins to drop again for higher interaction rates. As stated before, this can be attributed to overlap of events. This result confirms that event-based treatment is inadequate for realistic detector simulation at high event rates, but also that it is necessary to improve the existing time-based algorithms.

Note that the reconstruction efficiency does not exceed some $22\,\%$, even at interaction rates where no event overlap effects are present. This low efficiency is caused by a number of factors, mainly the inability of current tracking algorithm to reconstruct secondary decay vertices. Furthermore, the efficiency here is lowered by the online filter, which is designed to filter out background events but also erroneously rejects a sizeable portion of signal events.

4.2 EMC clustering

Photons, electrons and positrons can be fully stopped in the EMC, depositing their energy by initiating a particle shower in the scintillation crystal. These showers can extend into multiple crystal units, leaving signals in the EMC in the form of clusters. Decays which include these particles in their final states, such as $\bar{p}p \rightarrow e^+e^-$, $\bar{p}p \rightarrow e^+e^-\pi^0(\rightarrow \gamma\gamma)$, and $\bar{p}p \rightarrow J/\psi(\rightarrow e^+e^-)\pi^+\pi^-$ can be identified with EMC cluster information.

In the simulations described so far, event reconstruction is done using full information from all available subdetectors. However, it appears that for some channels, it is better to use only information from the EMC. In this case no tracking is done, and events are reconstructed solely using information from found EMC clusters (e.g. cluster energy, cluster polar angle). This was achieved effectively by only combining the neutral particle candidates in the analysis stage, and no charged candidates. See figure 4.4 for a flowchart visualisation the time-based event reconstruction process with EMC clusters. In this work, the default cluster finding task in PandaRoot is used.

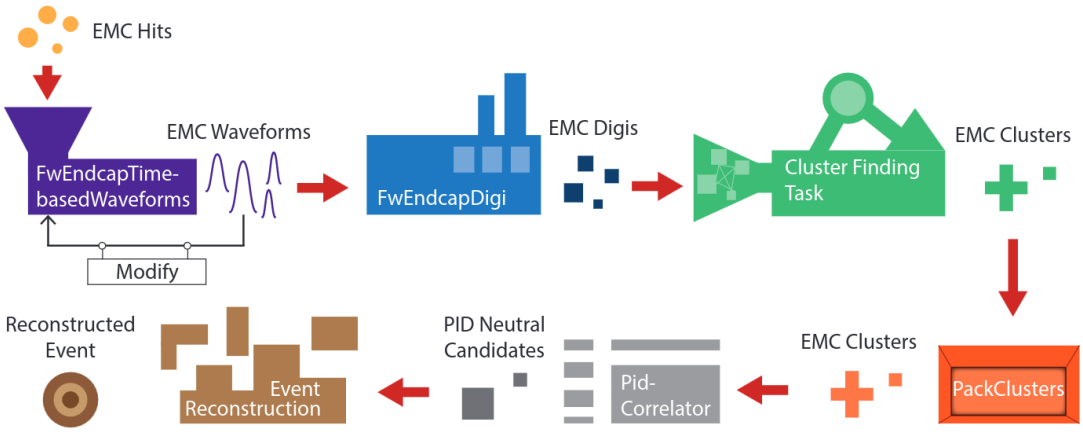

Figure 4.4: Steps in event reconstruction with EMC clusters. First, the hits in the EMC resulting from the propagation stage are converted to EMC waveforms including noise and pile-up effects. The waveforms are subsequently digitised, producing digis on which cluster finding can be performed. The found clusters are repacked and sorted to correct their timestamps for their flight time. Then, the PndPidCorrelator task forms neutral particle candidates out of the clusters, with PID likelihoods. In the analysis stage, particle candidates are recombined into full events. Chart taken from [10].

In this section, reconstruction quality of the three aforementioned channels is investigated. Invariant mass reconstruction based on EMC cluster information is compared to reconstruction with both EMC clusters and charged particle tracks.

4.2.1 Results

Time-based simulations of 10,000 signal events were done for each of the three channels $\bar{p}p \rightarrow e^+e^-$, $\bar{p}p \rightarrow e^+e^-\pi^0(\rightarrow \gamma\gamma)$, and $\bar{p}p \rightarrow J/\psi(\rightarrow e^+e^-)\pi^+\pi^-$. The events were simulated at an interaction rate of $2\,\mathrm{kHz}$ and with online filtering and Kalman filtering applied before the analysis stage. The reconstructed invariant mass spectra of the $\bar{p}p$ or J/ψ systems for each channel are compared to the standard configuration in which both the EMC and tracking detectors are used. In the latter case, tracking is done with the BarrelTrackFinder task (i.e. the standard tracking algorithm of PandaRoot). See figures 4.5 through 4.7.

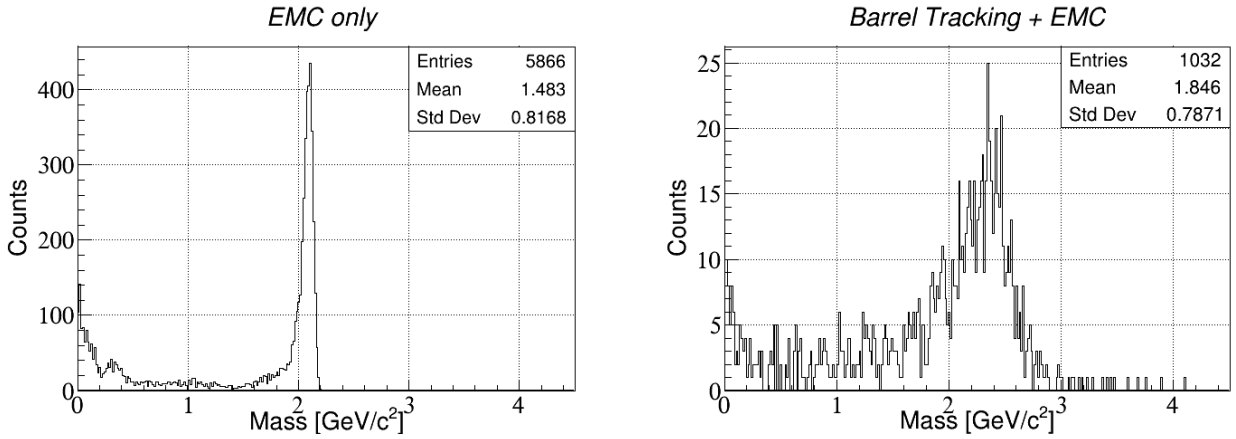

Figure 4.5: Reconstructed invariant mass spectrum of the $\bar{p}p$ system in the channel $\bar{p}p \rightarrow e^+e^-$ with only EMC information (left), and the standard EMC + tracking configuration (right).

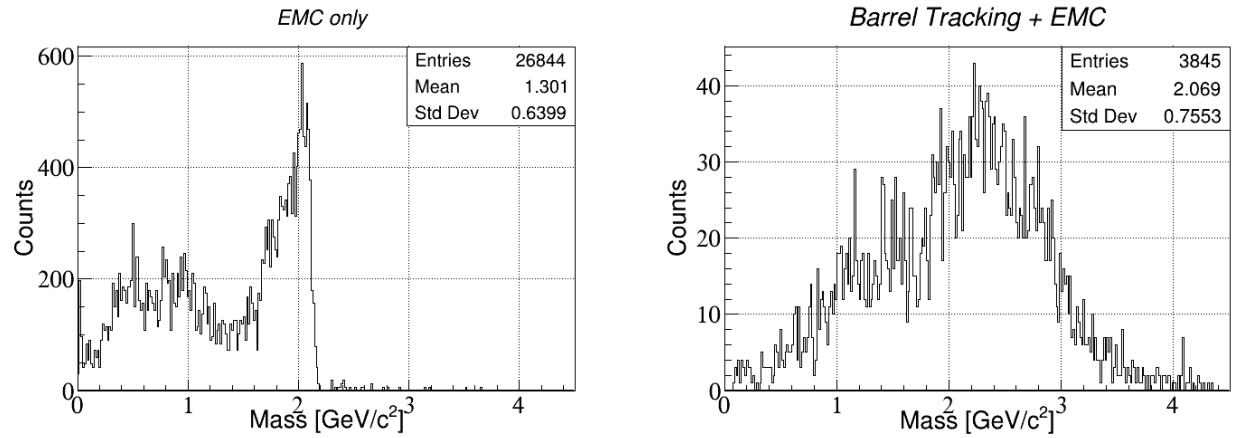

Figure 4.6: Reconstructed invariant mass spectrum of the $\bar{p}p$ system in the channel $\bar{p}p \rightarrow e^+e^-\pi^0$ with only EMC information (left), and the standard EMC + tracking configuration (right).

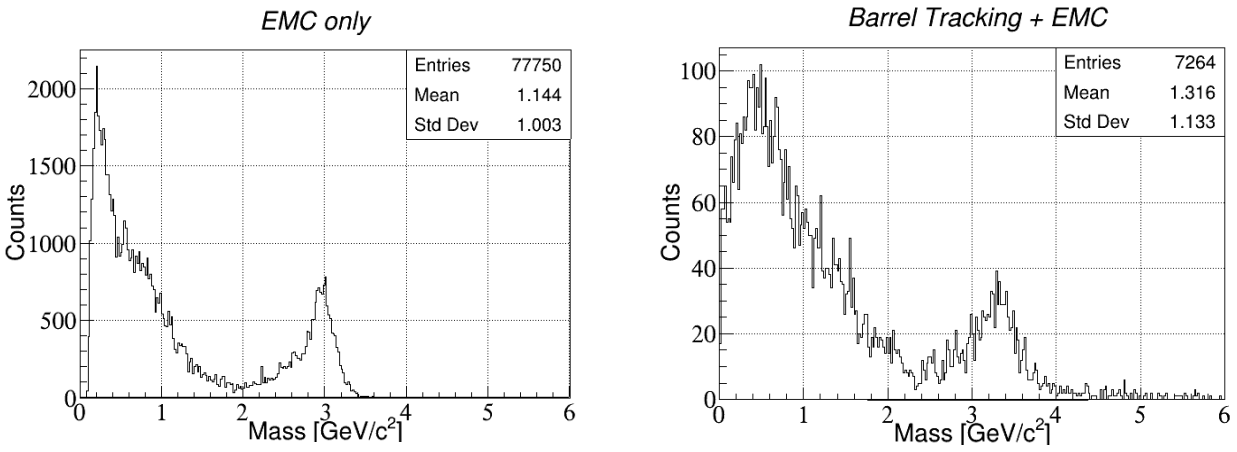

Figure 4.7: Reconstructed J/ψ invariant mass spectrum in the channel $J/\psi \to e^+e^-$ with only EMC information (left), and the standard EMC + tracking configuration (right).

For reference, see the invariant mass distributions included in appendix A. These are MC-truth matched candidates, so they do not contain misreconstructed invariant masses. The $\bar{p}p$ spectra obtained from simulations in this work would be expected to look like those, if the simulations are done with sufficient statistics and efficient reconstruction algorithms.

Comparing the left to the right hand spectra in figure 4.5, a substantial broadening of the peak is observed when tracking is introduced. The peak should be centred at $E_{\text{cm}} = 2.256\,\text{GeV}$, as is the case when tracking is done, but unlike in the case where only the EMC is used. This is because the electrons/positrons sometimes escape the EMC crystals, depositing only a certain fraction of their energies, leading to a systematic underestimation of the total final state energy of about $10\,\%$. This effect could however easily be accounted for with an energy calibration. Nevertheless, since the observed peak is narrower when no tracks are used, introducing tracking makes energy reconstruction less efficient.

A similar difference can be seen when comparing the spectra in figure 4.6. The peak in the spectrum on the right is broader than the one in the spectrum obtained for the channel $\bar{p}p \to e^+e^-$. This could be related to the fact that the two photons into which the neutral pion decays, will be reconstructed with poor momentum resolution. If the photons are not well-reconstructed, the electron-positron pair can be misidentified as a $\bar{p}p \to e^+e^-$ event with reduced energy. This could explain the broadening to the left of the peaks in the $\bar{p}p \to e^+e^-\pi^0$ channel. The number of counts in the left spectrum is inflated by combinatorics, but judging by the width of the peak, events in this channel are reconstructed more efficiently without tracking.

In figure 4.7, the J/ψ reconstructed invariant masses in the channel $\bar{p}p \to J/\psi(\to e^+e^-)\pi^+\pi^-$ are compared. To reconstruct the full decay tree would require reconstruction of the charged pion tracks, which would fail without tracking information. The expected result would be similar to the spectrum in figure 4.1 but with lower relative peak content due to the generally poorer reconstruction efficiency of this channel compared to the channel with muons in its final state (the dedicated muon detector aids that channel's reconstruction considerably). The difference between the spectra in figure 4.7 is not as substantial as for the other two chan-

nels, but the fact that introducing tracking does not enhance the reconstruction efficiency is nonetheless an indication that the applied tracking algorithms do not work as intended.

Note that this effect is not merely some deficiency of time-based algorithms. See the same comparison in event-based simulation mode in figure 4.8. Clearly tracking currently still works better in event-based simulation, but the efficiency lost by introducing tracking is greater in the time-based case.

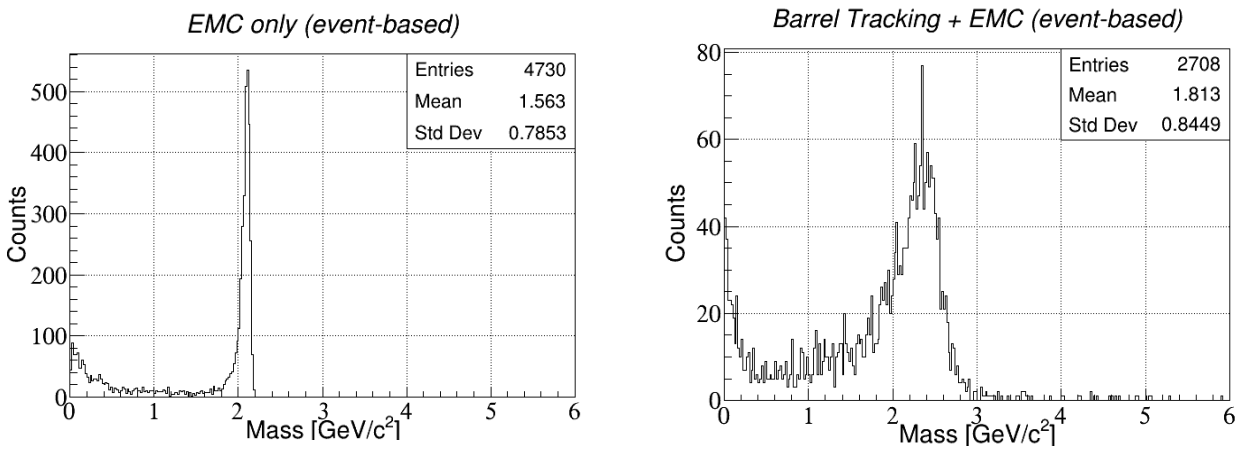

Figure 4.8: Reconstructed invariant mass spectra of the $\bar{p}p$ system in the channel $\bar{p}p \to e^+e^-$ with only the EMC (left), and EMC + tracking detectors (right). The events were simulated in event-based mode instead of time-based simulation mode.

The above results were unexpected. In principle, supplementing found clusters with tracking information should lead to better event reconstruction, as found charged tracks provide better momentum resolution and in some cases PID information. In the PID stage, a correlation check is done between charged track candidates and EMC clusters. Establishing such a correlation should help to more accurately reconstruct the kinematic parameters of e.g. electrons/positrons. The fact that the above results show that using only EMC cluster information improves event reconstruction in these channels can only mean that something is seriously wrong with the BarrelTrackFinder. Apparently the reconstructed track momenta are so poorly estimated that they are less accurate than the momenta reconstructed based only on cluster parameters, leading to a broader invariant mass peak. Something must be going wrong in the track finding process, leading to a substantial fraction of found tracks being false reconstructions. Either too many found tracks are false, or the clusters are matched with the wrong tracks in the PndPidCorrelator task (or both, with the latter being the result of the former). Tracking and further defects of the BarrelTrackFinder will be the subject of the next section.

4.3 Tracking with hyperons

As it was concluded in the previous sections that there is room for improvement in the area of track reconstruction, a new type of tracking algorithm was investigated. One major shortcoming of the BarrelTrackFinder is its inability to find secondary tracks. Because of the resulting loss of information, event reconstruction efficiencies remain low (as low as 2% for

$\bar{p}p \rightarrow \Lambda^0\bar{\Lambda}^0$ and the highest being 33% for $\bar{p}p \rightarrow e^+e^-\pi^0$). Therefore, a newly developed secondary track finding algorithm was investigated, described in the following section.

4.3.1 The ApolloniusTripletTrackFinder

The *ApolloniusTripletTrackFinder* is a newly developed algorithm that finds secondary tracks by making use of the isochrone information from the STT. STT hits come in the form of isochronous circles in the xy-plane to which the corresponding particle track is tangent (see section 2.2.1). Similarly to the existing primary tracking algorithm *HoughTrackFinder* [23], it applies the problem of Apollonius (i.e. finding a circle that is tangent to three given circles) to fit a circle on triplets of STT hits, and subsequently applies a Hough transform to all the possible circles to find the most probable track parameters. A preselection of STT hits is made to reduce combinatorics, as the runtime must be kept low since the algorithm is intended for online use. See [23] for a detailed description.

With its secondary track finding capabilities, this algorithm is expected to improve the quality of reconstruction especially for certain physics channels. The hyperons in the channel $\bar{p}p \rightarrow \Lambda^0(\rightarrow p\pi^-)\bar{\Lambda}^0(\rightarrow \bar{p}\pi^+)$ are relatively long-lived ($\tau_{\Lambda^0} = 0.26\,\mathrm{ns}$ [24]) and typically travel distances in the order of centimeters, sometimes tens of centimeters, before decaying. In this way secondary tracks are created outside the barrel region of the detector, where the BarrelTrackFinder algorithm cannot find them. For reference, the inner radius of the STT is $15\,\mathrm{cm}$, making information from this subdetector especially valueable for reconstructing hyperon decay vertices. Furthermore, the algorithm is presently only compatible with event-based simulation mode, and has not yet been adapted to time-based mode.

At present, the Apollonius tracking algorithm lacks the ability to reconstruct the z-components (longitudinal components) of track positions and momenta. Therefore an additional PandaRoot task was used to find the 'ideal' z-components of the hits by accessing their Monte Carlo-truth information (i.e. the z-components of the hits as they were generated in the simulation stage), *IdealPzFinder*. In this way it is possible to still assess the performance of the algorithm, though it must be noted that it is not entirely realistic.

4.3.2 Combining tracking algorithms

In order to make optimal use of the secondary track finding capabilities of the ApolloniusTripletTrackFinder, it was adapted to be used in tandem with the BarrelTrackFinder. This was realised in the following way. First, BarrelTrackFinder is applied to all digitised hits of the simulated events, and the tracks it reconstructs are stored in a branch. Then, the so-called *UnassignedHitsTask* is employed to find the digis that were not used by the BarrelTrackFinder to reconstruct any tracks. Subsequently, the ApolloniusTripletTrackFinder (with IdealPzFinder) is applied to the unassigned hits and the resulting tracks are merged with the Barrel tracks to be saved in a final branch. Following this tracking procedure, an event-based simulation of 20,000 events of the channel $\bar{p}p \rightarrow \Lambda^0\bar{\Lambda}^0$ events was performed. To gauge the performance of the algorithm, it was chosen to look at the reconstructed invariant masses of the $\bar{p}p$ system and to do a full MC-truth match. This entails that the reconstructed systems are checked with the MC-generated systems, and only those that match are kept. To compare the combined tracking algorithms with the original BarrelTrackFinder, this proce-

dure was repeated with the same digis, but using only the BarrelTrackFinder for tracking. See figure 4.9 for a comparison between the invariant mass spectra reconstructed with barrel tracking and combined tracking. Note that in both cases, just like in the standard procedure, full information from both the tracking systems and EMCs was used.

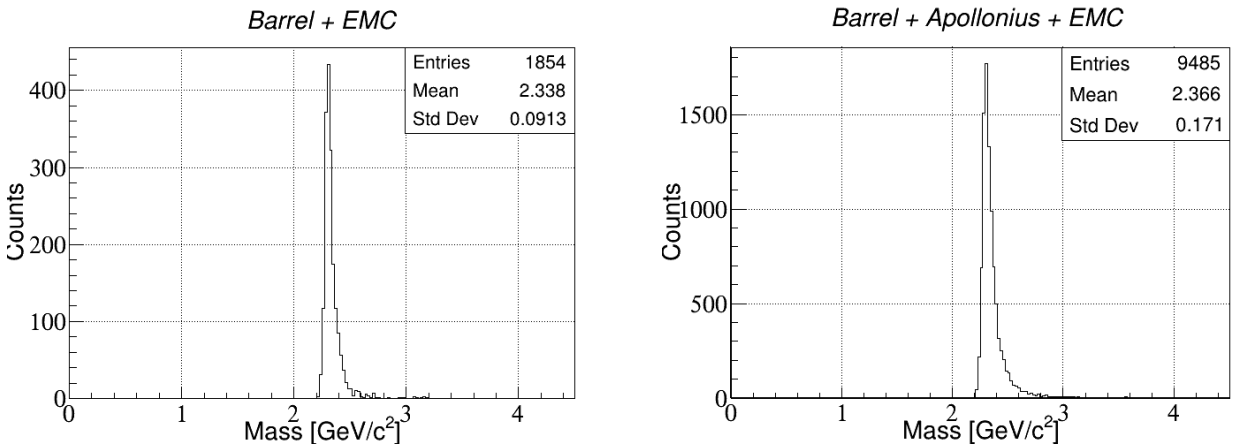

Figure 4.9: Reconstructed invariant mass spectra of the $\bar{p}p$ system in the channel $\bar{p}p \to \Lambda^0\bar{\Lambda}^0$ (20,000 events) after a full MC-truth match. Tracking was performed with the standard (BarrelTrackFinder) algorithm (left), and combined (BarrelTrackFinder + ApolloniusTripletTrackFinder) algorithms (right). EMC cluster information is also used in both cases.

The increase in the number of reconstructed $\bar{p}p$ candidates from 1854 to 9485 (out of 20,000) suggests a significant improvement in track reconstruction efficiency. The number of tracks found by the BarrelTrackFinder was 57,728. The ApolloniusTripletTrackFinder managed to reconstruct an additional 49,335 tracks, totalling 107,063 tracks for the combined tracking algorithms. The structure of the peaks does not seem to change, and has the expected shape like the spectrum shown in appendix A, figure A.1.e. Note that no Kalman filtering was applied in either case. The event reconstruction efficiency can be defined as $\varepsilon_{\text{reco}} = S_{\text{MCrec}}/S_0$. S_{MCrec} is the number of reconstructed MCtruth-matched signal events, and S_0 is the number of simulated signal events. When no secondary tracking is done, the reconstruction efficiency amounts to $\varepsilon_{\text{reco}} = 1854/20,000 = 9.3\,\%$. When secondary tracks are included, the efficiency is $\varepsilon_{\text{reco}} = 9485/20,000 = 47.4\,\%$. This result shows that much can be gained in this channel from secondary track information. Besides adding the secondary track finder, another reason the efficiency improved compared to the referenced work, is that Kalman filtering was not applied here. See the next section.

4.3.3 Kalman filter performance

A Kalman Filter is commonly applied to the found tracks, in a separate macro after the reconstruction stage. It is an iterative track fitting algorithm that refines track momentum precision, which should lead to a higher signal-to-noise ratio. This in principle improves the final event reconstruction efficiency [17]. See point 3 in section 3.1. However, it was discovered that applying a Kalman filter can in fact reduce the event reconstruction efficiency instead of improving it. See the comparison in figure 4.10. These are reconstructed invariant mass spectra of $\bar{p}p$ candidates in the channel $\bar{p}p \to \Lambda^0\bar{\Lambda}^0$ (20,000 events) after a full MC-truth match. Tracking was done with the (standard) BarrelTrackFinder, and in the left hand

figure Kalman filtering was not applied. In the right figure, Kalman filtering was applied. A lower peak content is observed when Kalman filtering is done. When applied to events reconstructed with combined tracking algorithms, the final number of reconstructed $\bar{p}p$ candidates is reduced by almost a whole order of magnitude (figure 4.11). In each of these cases, EMC cluster information was also used for event reconstruction.

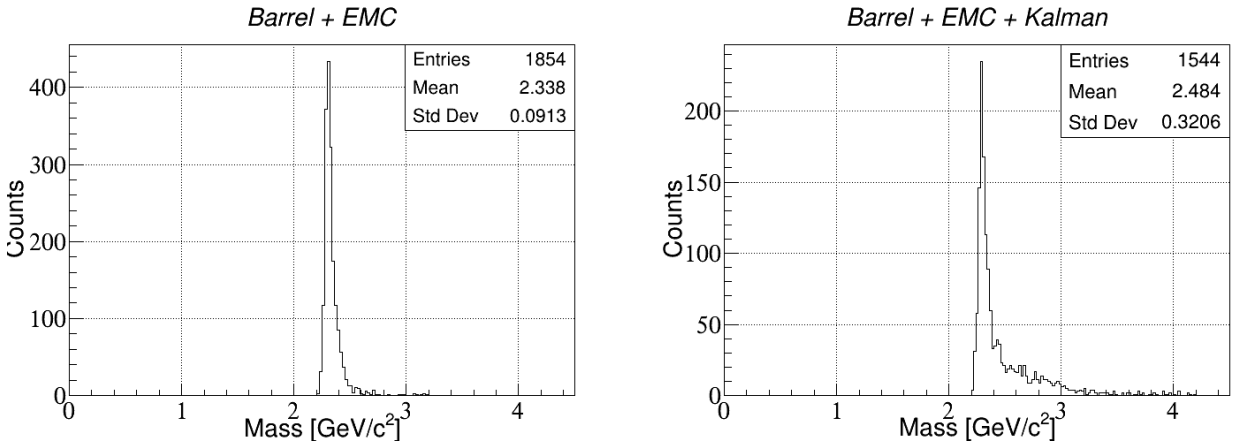

Figure 4.10: Reconstructed invariant mass spectra of the $\bar{p}p$ system in the channel $\bar{p}p \to \Lambda^0\bar{\Lambda}^0$ (20,000 events) after a full MC-truth match. Tracking with BarrelTrackFinder, and Kalman filtering not applied (left), Kalman filtering applied (right).

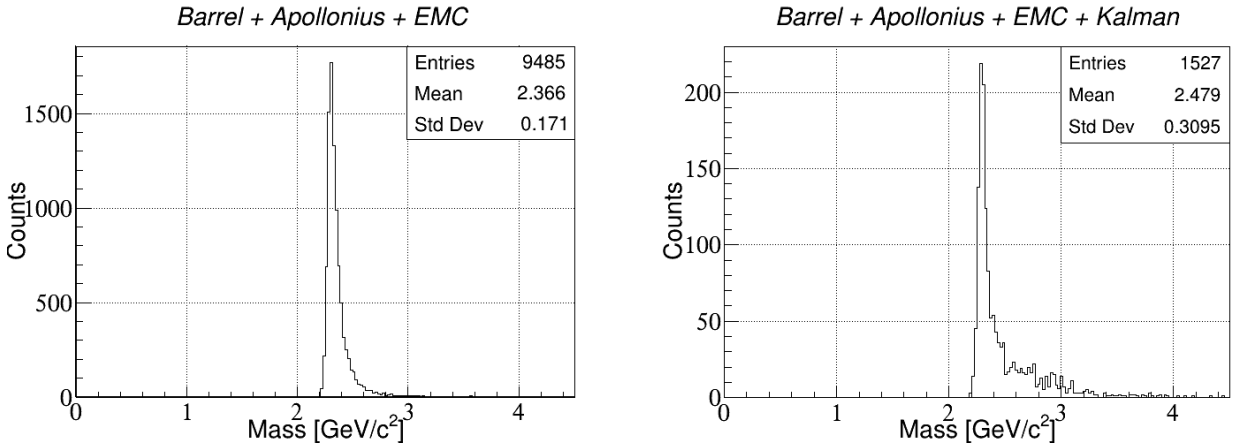

Figure 4.11: Reconstructed invariant mass spectra of the $\bar{p}p$ system in the channel $\bar{p}p \to \Lambda^0\bar{\Lambda}^0$ (20,000 events) after a full MC-truth match. Tracking with combined algorithms BarrelTrackFinder and ApolloniusTripletTrackFinder, and Kalman filtering not applied (left), Kalman filtering applied (right).

It appears that the Kalman filter algorithm is not suited to fitting the secondary tracks found by the ApolloniusTripletTrackFinder, discarding them all. Moreover, the shape of the spectrum changes when the Kalman filter is applied. See the added structure to the right side of the peaks in the right hand spectra of figures 4.10 and 4.11. This additional structure indicates that the Kalman filter systematically fits some tracks wrongly, as they end up outside the peak region with an overestimated invariant mass. Since this structure appears both with and without including secondary tracks, this defect of the Kalman filter is not merely a

problem of incompatability with the ApolloniusTripletTrackFinder. Whether this misfitting is limited to this type of physics channel is not yet clear.

4.3.4 Online filter performance

The performance of the online filter task, introduced in section 3.3, in response to events reconstructed by combined tracking algorithms was investigated for the channel $\bar{p}p \rightarrow \Lambda^0(\rightarrow p\pi^-)\bar{\Lambda}^0(\rightarrow \bar{p}\pi^+)$. Compared to the other benchmark channels, its signal and background profiles are more difficult to distinguish. Multiple filter criteria are applied to the events of this channel, as listed in section 3.3.

As before, 20,000 signal events were simulated and digitised, and barrel tracking was done to obtain one set of reconstructed tracks, and the combined barrel- and Apollonius algorithms were applied to the same digitised hits to obtain another set of reconstructed tracks. Full EMC information was used in both cases. The online filter algorithm was subsequently applied to both sets of events. No Kalman filtering was done, and after physics analysis the invariant mass spectra of the $\bar{p}p$ candidates were obtained (figure 4.12).

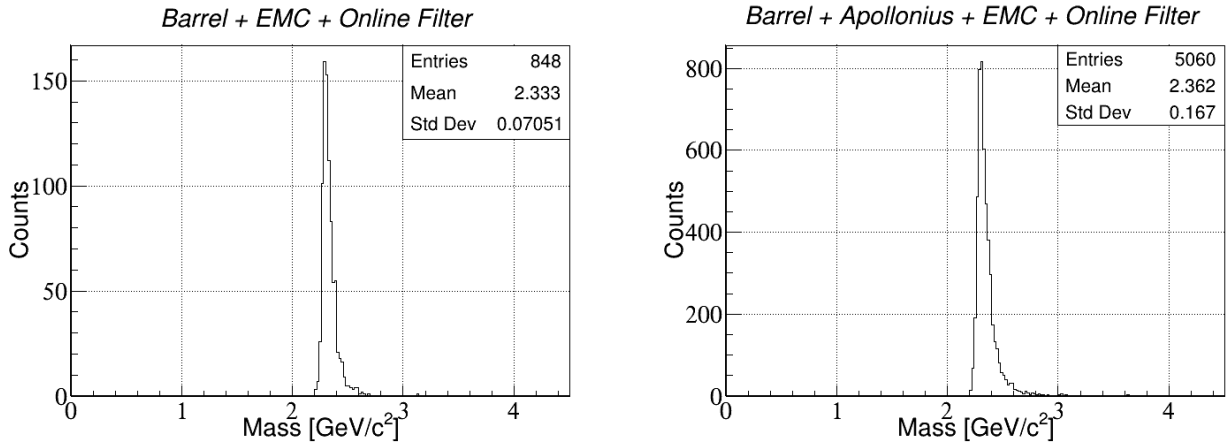

Figure 4.12: Reconstructed invariant mass spectra of the $\bar{p}p$ system in the channel $\bar{p}p \rightarrow \Lambda^0\bar{\Lambda}^0$ (20,000 signal events) after a full MC-truth match. In both cases online filtering was applied. In the first case (left), tracking was performed with the barrel tracking algorithm. In the second case (right), tracking was performed with combined tracking algorithms (BarrelTrackFinder + ApolloniusTripletTrackFinder). Kalman filtering was not applied in both cases.

Comparing these spectra to the ones in figure 4.9, one observes that the online filter discards a sizeable fraction of reconstructed events. This fraction can be defined as the filter efficiency $\varepsilon_{\text{filt}} = S_{\text{filt}}/S_{\text{MCrec}}$. Here one compares the number of signal events reconstructed with filtering applied, S_{filt}, and without, S_{MCrec}. When no secondary tracking is done, the filter efficiency is therefore $\varepsilon_{\text{filt}} = 848/1854 = 45.7\,\%$. With secondary tracking added, the filter efficiency is $\varepsilon_{\text{filt}} = 5060/9485 = 53.4\,\%$. In both cases, about half of the signal events survive the online filter with the selected criteria. The filter efficiency for this channel was benchmarked by Viktor Rodin as $\varepsilon_{\text{filt}} = 26.7\,\%$ (with Kalman filtering and no secondary track finding). The increased filter efficiency could be caused by the absence of the Kalman filter. Since the Kalman filter misfits tracks, it is possible that the resulting event parameters then no

longer meet the filter criteria. The obtained filter efficiencies of tens of percents are acceptable if the background suppression factor requirement of two to three orders of magnitude is met.

In a similar fashion, 20,000 background events were simulated and reconstructed with both tracking configurations. The background suppression factor f_{sup} is defined to be the number of background events which passed the filter, B_{filt}, relative to the number of simulated background events, $B_0 = 20,000$: $f_{\text{sup}} = B_0/B_{\text{filt}}$. Note the difference in definition of the background suppression factor from Viktor Rodin's PhD thesis, p.141 [21]. This definition was chosen because without applying Kalman filtering, combinatorics inflate the counts in the reconstructed invariant mass spectra. In the case of signal events, this problem can be circumvented by MC-truth matching, but this is not possible for background events. The obtained suppression factors are listed in table 4.1, along with the aforementioned reconstruction- and filter efficiencies:

	$\varepsilon_{\text{reco}}$ [%]	$\varepsilon_{\text{filt}}$ [%]	f_{sup}
Barrel+EMC	9.3	45.7	625
Barrel+Apollonius+EMC	47.4	53.4	187

Table 4.1: Final comparison between barrel tracking and combined tracking. Obtained after simulation of 20,000 $\bar{p}p \rightarrow \Lambda^0\bar{\Lambda}^0$ signal events and 20,000 background events (no mixing).

The background suppression factor is lower for combined tracking than for just barrel tracking. This would result in a lower data reduction factor. Part of this difference is caused by the increased number of reconstructed tracks in the combined tracking case. Therefore there are more (background) events which by chance meet the criteria to pass the filter. In addition, the choice of the used filter criteria was based on simulations in which event reconstruction was done without secondary tracking. Perhaps better filter criteria can be contrived, tailored for a combined tracking configuration. In any case, since the suppression factor is of the desired order of magnitude, the online filter strategy is viable also when combined track reconstruction algorithms are used.

The reconstruction efficiency for this channel was benchmarked in Viktor Rodin's work as $\varepsilon_{\text{reco}} = 2.0\,\%$ [21]. This efficiency was low mainly because of the reason that secondary track finding was not implemented, causing the reconstruction algorithms to miss information. Evidently, this efficiency can be increased significantly by implementing secondary track finding and disabling Kalman filtering.

In conclusion, reconstruction of the $\bar{p}p \rightarrow \Lambda^0\bar{\Lambda}^0$ channel can be improved by introducing secondary vertex reconstruction and by not applying a Kalman filter. This lead to a reconstruction efficiency of $\varepsilon_{\text{reco}} = 47.4\,\%$. Furthermore, the online filter requirements can be met also when track finding is done with the combined BarrelTrackFinder + ApolloniusTripletTrackFinder, as the background suppression rate is of the appropriate order of magnitude and the filter efficiency was increased. For future work, it could be worthwhile to extend the BarrelTrackFinder with the ability to find secondary tracks, and to find the origin of its inefficiencies described in section 4.2. Furthermore, a secondary track finding algorithm compatible with time-based simulation mode should be developed.

5 Summary and conclusions

$\overline{\mathrm{P}}$ANDA is a planned particle physics experiment aspiring to gain insight into various hadronic phenomena. With its high-luminosity antiproton beam creating a gluon-rich environment, $\overline{\mathrm{P}}$ANDA offers unique circumstances to study hadron formation, exotic states, hypernuclei, and more. In order to cope with high expected interaction rates (up to $2\,\mathrm{MHz}$ during phase-1 and $20\,\mathrm{MHz}$ during phase-2) at $\overline{\mathrm{P}}$ANDA, while adhering to its physics goals, a triggerless data acquisitions system (tDAQ) is envisioned. To reduce the output data rate, this system will perform real-time event selection using software. A dedicated simulation environment called PandaRoot is used to perform Monte Carlo event generation, digitisation, event reconstruction and physics analysis. With interaction rates in the MegaHertz regime, effects such as signal pileup and overlap become prominent, requiring reconstruction algorithms to take timestamps into account. Such a time-based simulation mode is under development in PandaRoot, but still needs improvement. In this work, a number of improvements were made to the reconstruction efficiency of five benchmark channels.

The first result was related to the active time parameter in time-based simulation. This parameter was optimised for a number of values of the interaction rate ($2\,\mathrm{kHz}$ to $2\,\mathrm{MHz}$), revealing the dependance of the reconstruction efficiency on active time in the channel $\bar{p}p \rightarrow J/\psi(\rightarrow \mu^+\mu^-)\pi^+\pi^-$.

It was found that the benchmark channels with electrons/positrons or gammas in their final states can be reconstructed better using only EMC cluster information, and not doing any tracking. This result is rather surprising and points to flawed tracking algorithms.

The most difficult benchmark channel to reconstruct is $\bar{p}p \rightarrow \Lambda^0(\rightarrow p\pi^-)\bar{\Lambda}^0(\rightarrow \bar{p}\pi^+)$. It was found that reconstruction of these events can be significantly improved by applying the standard track reconstruction algorithm in parallel with a new secondary track finding algorithm, the ApolloniusTripletTrackFinder. This algorithm is currently incompatible with time-based simulation mode, and so the simulations of this channel were done in event-based mode. It was shown that applying a Kalman filter to fit these tracks results in a worse reconstruction of the $\bar{p}p$ invariant mass. This is another surprising result. In the future the cause of the Kalman misfitting should be investigated. Lastly, the performance of the online filter task was assessed with the combined tracking configuration and without applying Kalman filtering. The filter efficiency and the background suppression rates are within the desired orders of magnitude, and therefore the online filter stategy was deemed viable for combined tracking.

In the future, the existing tracking algorithms in PandaRoot must be improved. To efficiently reconstruct hyperon decays, it is advisable to extend the BarrelTrackFinder with secondary tracking abilities, or perhaps replace it altogether. Moreover, a time-based compatible secondary track finding algorithm should be developed. In general, time-based reconstruction algorithms need much work to be able to handle the $20\,\mathrm{MHz}$ event-rate expected for phase 2. Furthermore, the exact cause of the defects of the Kalman filter demonstrated in section 4.3.3 must be tracked down, and it must be ensured to improve the momentum resolution of all tracks.

Acknowledgments

"There are decades where nothing happens; and there are weeks where decades happen."

— Lenin

I would like to thank my primary supervisor, Myroslav, for offering me this project and for all the useful feedback. It took me some extra time to finish this thesis (hence the above quotation), so thanks for your patience.

Next, I wish to thank Viktor Rodin. My project was done to complement part of your PhD research, and I'm glad some of my results were useful to you, despite containing some inconvenient truths ;). I learned many new things during this project, and I owe you much gratitude for all the times you've helped me with technical problems and interpretation. It was an honour to be one of your paranymphs at your promotion ceremony and I wish you all the best with your new job.

Many thanks to Anna Alicke from the Jülich group. You were very patient in explaining how to use your tracking algorithm, the ApolloniusTripletTrackFinder. I struggled with it quite a bit, but with your help it worked in the end. One time you even spent multiple hours debugging the code with me via text chat! Thank you very much for your help.

I thank everyone from the nuclear energy group for all the interesting presentations and discussions during our group meetings. In particular I thank Nasser for his valuable feedback on my work (and all the political discussions at lunch, of course).

Lastly, special thanks to my office mates Ali and Geet. We had a lot of fun both in and outside the office (Geet's dahl and biryani are unmatched).

Appendices

A Invariant mass distributions of the benchmark channels

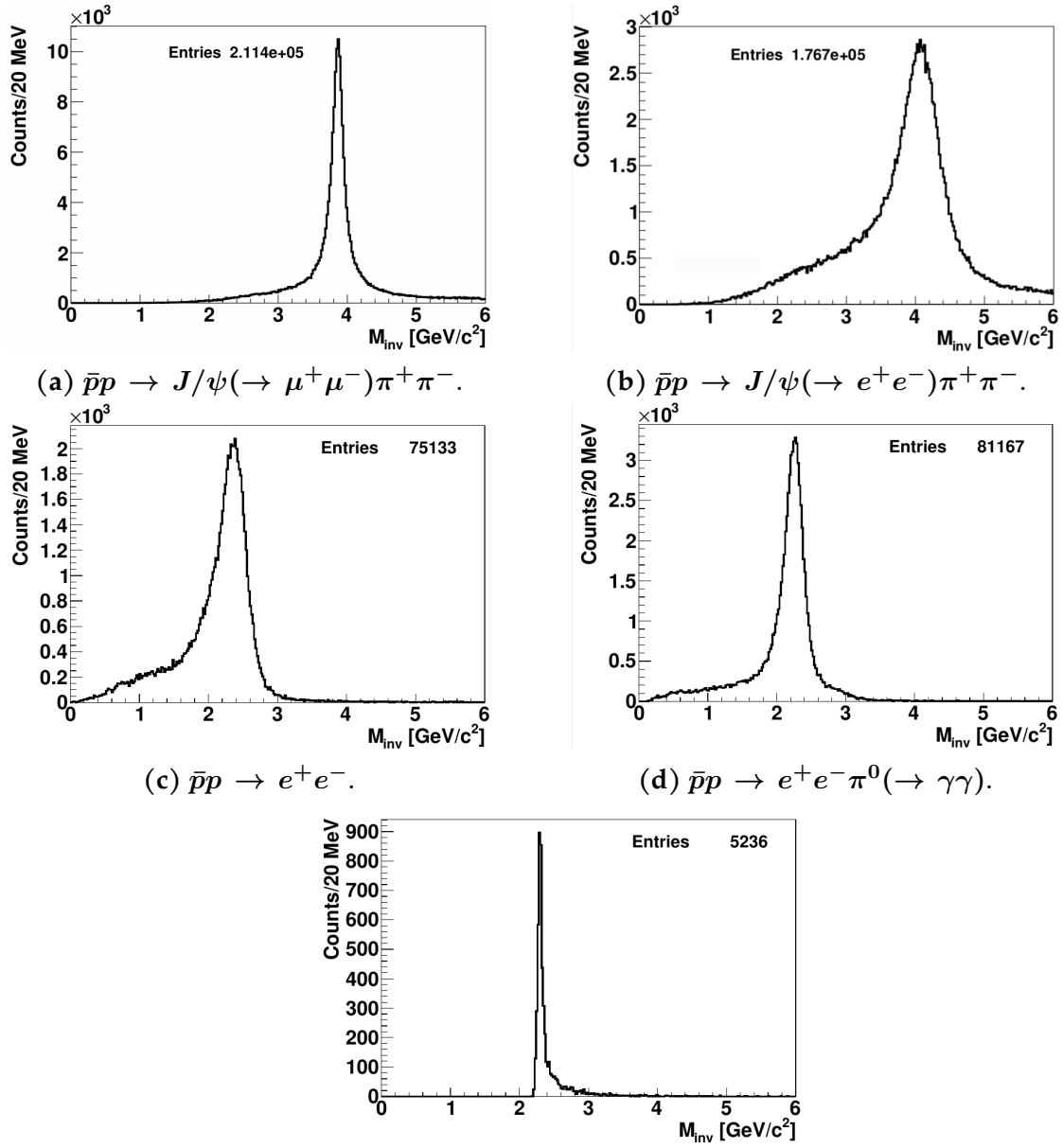

(a) $\bar{p}p \rightarrow J/\psi(\rightarrow \mu^+\mu^-)\pi^+\pi^-$.

(b) $\bar{p}p \rightarrow J/\psi(\rightarrow e^+e^-)\pi^+\pi^-$.

(c) $\bar{p}p \rightarrow e^+e^-$.

(d) $\bar{p}p \rightarrow e^+e^-\pi^0(\rightarrow \gamma\gamma)$.

(e) $\bar{p}p \rightarrow \Lambda^0(\rightarrow p\pi^-)\bar{\Lambda}^0(\rightarrow \bar{p}\pi^+)$.

Figure A.1: Invariant mass spectra of MC-truth matched $\bar{p}p$ candidates for the five benchmark channels. The number of simulated events was in each case 10^6. Taken from Viktor Rodin's PhD disseration [21].

Bibliography

[1] Barucca, G., et al. "PANDA Phase One: PANDA collaboration." The European Physical Journal A 57 (2021): 1-36.

[2] Belias, A. "FAIR status and the PANDA experiment." Journal of Instrumentation 15.10 (2020): 10001.

[3] Stockhorst, Hans, et al. "Stochastic cooling for the HESR at the GSI-FAIR complex." Proc. EPAC. 2006.

[4] Lehrach, A., et al. "Beam dynamics of the high-energy storage ring (HESR) for FAIR." International Journal of Modern Physics E 18.02 (2009): 420-429

[5] Schwarz, Carsten, and PANDA Collaboration. "The PANDA experiment at FAIR." Journal of Physics: Conference Series. Vol. 374. No. 1. IOP Publishing, 2012.

[6] PANDA Collaboration. "The Cluster-Jet Target and Developments for the Pellet Target." Technical Design Report for the PANDA Internal Targets (2012).

[7] Collaboration, P. A. N. D. A. "Technical design report for the: PANDA straw tube tracker." arXiv: 1205.5441 (2012).

[8] Moritz, Markus, et al. "The electromagnetic calorimeter for the PANDA target spectrometer." Journal of Physics: Conference Series. Vol. 1162. No. 1. IOP Publishing, 2019.

[9] Schepers, G. "Particle identification at PANDA, report of the PID TAG." PANDA Note, March (2009).

[10] Tiemens, Marcel. "Online Cluster-Finding Algorithms for the PANDA Electromagnetic Calorimeter." (2017)

[11] Panda Collaboration, et al. "Precision resonance energy scans with the PANDA experiment at FAIR: Sensitivity study for width

[12] Wiedner, Ulrich. "Future prospects for hadron physics at $\bar{P}$ANDA." Progress in Particle and Nuclear Physics 66.3 (2011): 477-518.

[13] Götzen, R. K. K., D. Kang, and F. Nerling. "Present Status of the PANDA Software Trigger." PANDA Internal Note (2014): 59-65.

[14] Spataro, Stefano. "Simulation and event reconstruction inside the PandaRoot framework." Journal of Physics: Conference Series. Vol. 119. No. 3. IOP Publishing, 2008.

[15] Lange, David J. "The EvtGen particle decay simulation package." Nuclear Instruments and Methods in Physics Research Section A: Accelerators, Spectrometers, Detectors and Associated Equipment 462.1-2 (2001): 152-155.

[16] Pi, Hong. "An event generator for interactions between hadrons and nuclei—FRITIOF version 7.0." Computer Physics Communications 71.1-2 (1992): 173-192.

[17] Frühwirth, Rudolf. "Application of Kalman filtering to track and vertex fitting." Nuclear Instruments and Methods in Physics Research Section A: Accelerators, Spectrometers, Detectors and Associated Equipment 262.2-3 (1987): 444-450.

[18] Frühwirth, R., and S. Frühwirth-Schnatter. "On the treatment of energy loss in track fitting." Computer physics communications 110.1-3 (1998): 80-86.

[19] Spataro, Stefano. "Event Reconstruction in the PandaRoot framework." Journal of Physics: Conference Series. Vol. 396. No. 2. IOP Publishing, 2012.

[20] Barucca, G., Davì, F., Lancioni, G. et al. PANDA Phase One. Eur. Phys. J. A 57, 184 (2021).

[21] Rodin, Viktor. "Performance studies for the trigger-less data acquisition of the PANDA experiment (phase-1)." (2023)

[22] Regina, Jenny, and Walter Ikegami Andersson. "Time-based reconstruction of hyperons at PANDA at FAIR." arXiv preprint arXiv:1910.06086 (2019).

[23] Alicke, Anna, Tobias Stockmanns, and James Ritman. "Track Finding for the PANDA Detector Based on Hough Transformations." EPJ Web of Conferences. Vol. 251. EDP Sciences, 2021.

[24] P.A. Zyla et al. (Particle Data Group), Prog. Theor. Exp. Phys. 2020, 083C01 (2020) and line shape measurements of the X (3872)." The European Physical Journal A 55 (2019): 1-18.